Nanoscale

PAPER

Highly flexible transparent self-healing composite based on electrospun core–shell nanofibers produced by coaxial electrospinning for anti-corrosion and electrical insulation

Cite this: DOI: 10.1039/c5nr04551g

Seongpil An,[a] Minho Liou,[a] Kyo Yong Song,[a] Hong Seok Jo,[a] Min Wook Lee,[b] Salem S. Al-Deyab,[c] Alexander L. Yarin*[a,b] and Sam S. Yoon*[a]

Received 8th July 2015,
Accepted 15th September 2015
DOI: 10.1039/c5nr04551g
www.rsc.org/nanoscale

Coaxial electrospinning was used to fabricate two types of core–shell fibers: the first type with liquid resin monomer in the core and polyacrylonitrile in the shell, and the second type with liquid curing agent in the core and polyacrylonitrile in the shell. These two types of core–shell fibers were mutually entangled and embedded into two flexible transparent matrices thus forming transparent flexible self-healing composite materials. Such materials could be formed before only using emulsion electrospinning, rather than coaxial electrospinning. The self-healing properties of such materials are associated with release of healing agents (resin monomer and cure) from nanofiber cores in damaged locations with the subsequent polymerization reaction filing the micro-crack with polydimethylsiloxane. Transparency of these materials is measured and the anti-corrosive protection provided by them is demonstrated in electrochemical experiments.

1. Introduction

Metal-framed structures such as buildings, bridges, and vehicles are inevitably vulnerable to corrosion induced by moisture in the air or rain, together with atmospheric oxygen. Thus, corrosion is an important issue that must be addressed to ensure the sustainability and reliability of metallic structures. According to a US federal report, the total estimated annual cost required to face the issue of corrosion was $276 billion.[1] In lieu of treating the corrosion issue directly, ceramics and polymer materials have been suggested as alternative structural materials. However, these are subject to micro-cracks by external shocks[2,3] that can result in catastrophic failure, which is worse than corrosion. The prevention of corrosion and micro-cracks is thus important for both the safety of human life and economic feasibility. For these reasons, various approaches have been proposed to protect structures from corrosion and micro-cracks. In one study, a corrodible substrate underwent surface modification with an anti-corrosion material.[4] However, this type of surface modification proved to be a temporary treatment, because corrosion eventually occurred through small cracks in the anti-corrosion material. As an alternative, the use of self-healing materials has been proposed; these form physical protective barriers as well as provide *in situ* repair or healing capabilities when the structures to which they are applied are damaged.[5–11]

Polydimethylsiloxane (PDMS) has been widely used because of its chemical stability in air, water, and even industrial chemicals.[12–14] In addition, PDMS is transparent and flexible; these properties offer significant advantages in uses in optical and electronic devices, such as displays, touch screens, solar cells, smart windows, and interactive electronics.

There are various methods of embedding self-healing agents in different materials and composites. Namely, microscopic capsules and core–shell nanofibers have been demonstrated as means to embed self-healing agents in different materials and composites. When a metal is in direct contact with a corrosive environment due to the presence of micro-cracks, the healing agents can be released from the capsules and/or nanofibers and undergo polymerization reaction due to the catalysts embedded in the surrounding matrix or cure released from separate capsules and/or nanofibers. As a result, the micro-cracks are filled with the polymerized material and the metal surface is protected again.[8,10,15–18] Notably, however, the approach based on capsule with healing agents suffers from high manufacturing cost, poor connections between capsules, and their non-uniform distribution in the surrounding matrix. In addition, the length scale of most capsules is in the range of tens of microns, which is structurally burdensome to carry and incommensurate with

[a]School of Mechanical Engineering, Korea University, Seoul 136-713, Republic of Korea. E-mail: ayarin@uic.edu, skyoon@korea.ac.kr
[b]Department of Mechanical and Industrial Engineering, University of Illinois at Chicago, Illinois 60607-7022, USA
[c]Petrochem. Research Chair, Department of Chemistry, College of Sci., King Saud University, Riyadh 11451, Saudi Arabia

the material characteristic scales, especially for vehicular applications in automobiles, tanks, and aircraft.

The approach based on core–shell nanofiber containing healing agents can circumvent the above-mentioned problems associated with capsules. First, the diameters of the fibers are in the range of a few hundred nanometers. Second, the fibers are entangled and thus inter-connected, which enables the efficient transport of healing agents through the three-dimensional network formed by the fibers.[6,9,19] Third, such fibers are much lighter than the aforementioned capsules, thus reducing the burden of the payload. Fourth, the fibers can become a part of highly transparent composites.[20,21]

Micro-fibers can be formed by melt blowing,[22] wet spinning,[23] force spinning,[24,25] solution blow spinning,[26,27] and electrospinning.[28] Herein, we fabricated core–shell nanofibers carrying a healing agent and curing catalysts separately inside the cores of the different nanofibers. These core–shell fibers were formed using coaxial electrospinning (co-electrospinning) of the core and shell materials from the core and the surrounding annular nozzle, in distinction from the previous works of this group, where similar core–shell fibers were formed using the emulsion electrospinning.[29,30] Although coaxial electrospinning has been widely reported in creating core–shell nanofibers with only one of the core or shell working fluids having electrospinnability, very limited publications investigated the usage of functional liquids as the core parts of core–shell nanostructures.[20,21,31–33] Once the core–shell fibers co-electrospun in the present work were cut open, the healing and curing materials were released, and underwent polymerization to form a protective layer.

2. Experimental

2.1. Materials

Three solutions were used to co-electrospin core–shell nanofibers containing either resin monomer or cure in the core. For the shell solution, polyacrylonitrile (PAN, M_w = 150 kDa) and *N*,*N*-dimethylformamide (DMF, 99.8%) from Sigma-Aldrich were used. An 8 wt% PAN solution in DMF was prepared by magnetic stirring for 24 h at room temperature. For the core solutions, either liquid dimethylvinyl-terminated dimethyl siloxane (resin monomer) or methylhydrogen dimethyl siloxane (curing agent, referred to henceforth as "cure"), both from i-Nexus, and *n*-hexane from Duksan Pure Chemicals were used. The two core materials (the resin monomer and the curing agent) could be released and start interacting only when the PAN shell has been torn. Then, polymerization of PDMS took place and healed the damaged place. In the corrosion test, an acetic acid solution and steel substrates were obtained from Wako Pure Chemical Industries.

2.2. Co-electrospinning of self-healing core–shell nanofibers

In the self-healing core–shell nanofibers, either the resin monomer, or the cure, were embedded in the core, while PAN formed the shell. Two syringes were used to simultaneously co-electrospin the resin monomer-PAN (R-PAN) and cure-PAN (C-PAN) nanofibers, which were simultaneously deposited on the drum collector (Fig. 1). A large-area self-healing nanofiber mat in which both R-PAN and C-PAN nanofibers were intertwined was formed. The flow rates of the core and shell components were controlled by using two syringe pumps (Legato 100, KDS); with the volumetric flow rates of 70 and 900 μL h^{-1}, respectively. In the case of the R-PAN solution, *n*-hexane was admixed with the liquid resin monomer in the volume ratio of 1 : 2 to enable stable co-electrospinning, which was impossible with the pure resin monomer. The DC voltage applied to both R-PAN and C-PAN solutions was 13 kV, and the distance between the nozzle and the substrate was 9 cm. The inner diameters of the core and shell nozzles were 0.61 (EFD 20 gauge) and 1.54 mm (EFD 14 gauge), respectively. Homogeneous deposition of the two types of core–shell nanofibers on the rotated collector was ensured by the identical volumetric flow rates and strengths of the electric field employed to form R-PAN and C-PAN nanofibers.

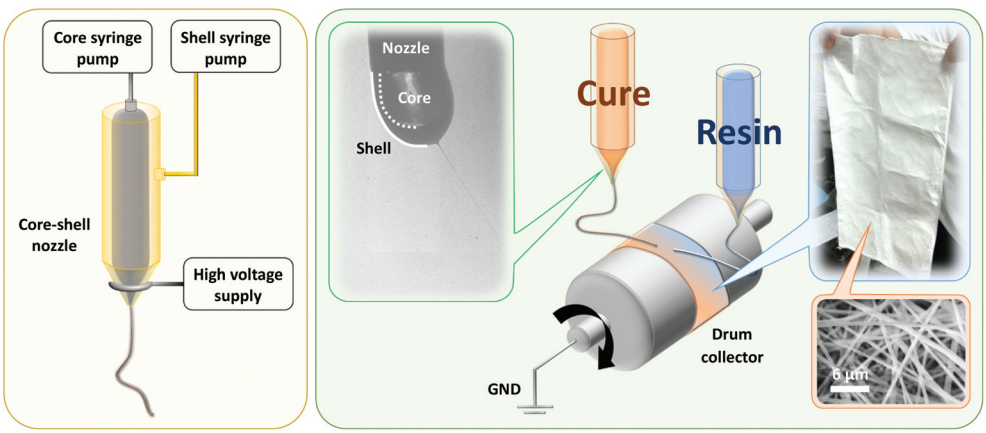

Fig. 1 Schematics of the coaxial electrospinning process. Detailed schematic of the core–shell nozzle (left). Schematic and the images of the cores–shell droplet issuing core–shell jets resulting in a large-area core–shell nanofiber mat on a drum collector in the co-electrospinning setup with two core–shell syringes (right).

2.3. Characterization

Images of the intact and ruptured self-healing core–shell nanofibers were obtained using scanning electron microscope (SEM, FE-SEM S-5000, Hitachi, Ltd). To identify the core–shell structure of the nanofibers, transmission electron microscope (TEM, JEM 2100F, JEOL Inc.) was used under the operating conditions of 200 kV.

Thermal Gravimetric Analysis (TGA) and Derivative Thermogravimetric Analysis (DTG) (SDT Q600, TA Instruments) were conducted at a flow rate of 100 mL min^{-1} of argon gas. All samples in the 1.5–1.9 mg weight range were heated from room temperature to 800 °C at a heating rate of 10 °C min^{-1}. To obtain the transmittance data of the self-healing core–shell nanofiber-embedded composite, indium tin oxide (ITO) glass (2.5 × 2.5 × 0.07 cm^3) was used as the substrate and a UV/VIS spectrophotometer (Optizen POP, MECASYS Co., Ltd) was used to identify the transmittance values.

An electrochemical test was conducted by applying the Scanning Vibrating Electrode Technique (SVET),[30,34,35] in which the electric current values were measured by a source meter (Model 2400, Keithley Instruments) and a field strength of 5 V was applied for 200 s.

3. Results and discussion

3.1. Co-electrospun self-healing core–shell nanofibers

Because all electric charges mostly accumulated on the outer surface of the Taylor cone of the shell, the flow rate of the core solution was significantly lower than that of the shell solution.[36] The velocity difference between the core and shell solutions generated a viscous force, which resulted in the entrainment of the core into the shell and formation of the core–shell fibers. According to Reznik *et al.*,[36] the ratio of the radii of the core and shell nozzles (r_{core}/r_{shell}) should be below 0.6, because multiple jets instead of a single core–shell jet are formed above this value. Accordingly, in the present experiment, the r_{core}/r_{shell} ratio was 0.4. The stable core–shell Taylor cone was maintained for many hours because of that and the fact that no polymerization reactions occurred between any single healing agent on the core and shell PAN solution in the shell.

Fig. 2a and b shows the SEM images of R-PAN and C-PAN nanofibers. The nanofibers are sufficiently uniform and no bead were observed. The diameter of the core–shell nanofibers is in the 300 to 350 nm range.

The presence of the core materials in the nanofibers was confirmed by pressing nanofibers that had been deposited on steel substrates with a tweezer. In Fig. 2c and d, the liquid core materials (the healing agents) are observed to have leaked after the nanofibers were ruptured. It should be emphasized that the liquid state of the core materials was maintained during the entire co-electrospinning process, even after solvent evaporation and precipitation and solidification of the shell.[37,38] To further corroborate the core–shell structure of the nanofibers, TEM images were obtained as shown in Fig. 3. The TEM samples were prepared by depositing nanofibers onto a copper grid for a few seconds. The interfacial boundary lines between the core and the shell are clearly visible in both R-PAN and C-PAN nanofibers. The whole core–shell and the core diameters of the R-PAN nanofiber are ~293 and ~189 nm, respectively, and in the C-PAN nanofiber, the whole core–shell and the core diameters are ~360 nm and ~195 nm, respectively.

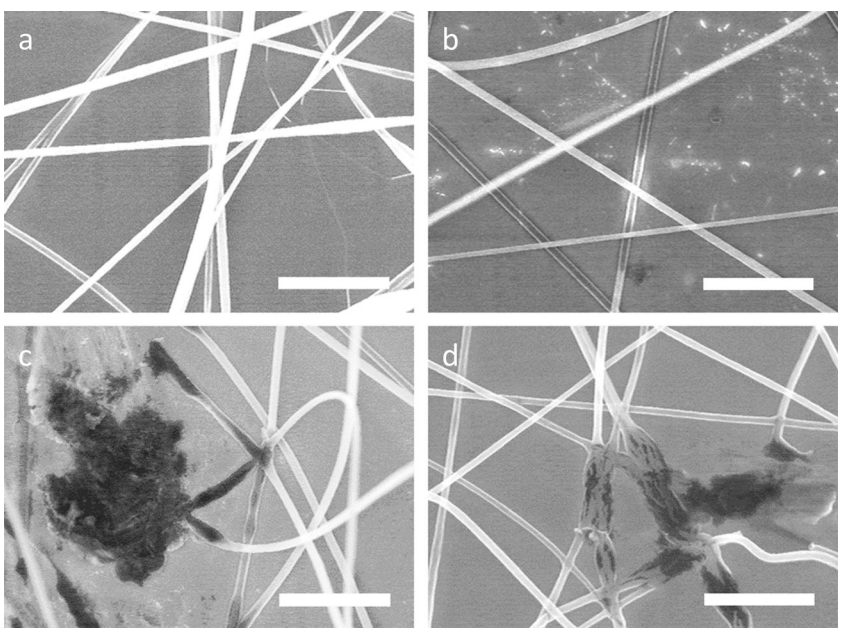

Fig. 2 SEM images of core–shell nanofibers. (a) R-PAN nanofibers, (b) C-PAN nanofibers, (c) ruptured R-PAN nanofibers, (d) ruptured C-PAN nanofibers. Nanofibers shown in panels (a) and (d) were ruptured using a tweezer to observe release of agent materials from the core. The scale bar is 6 μm.

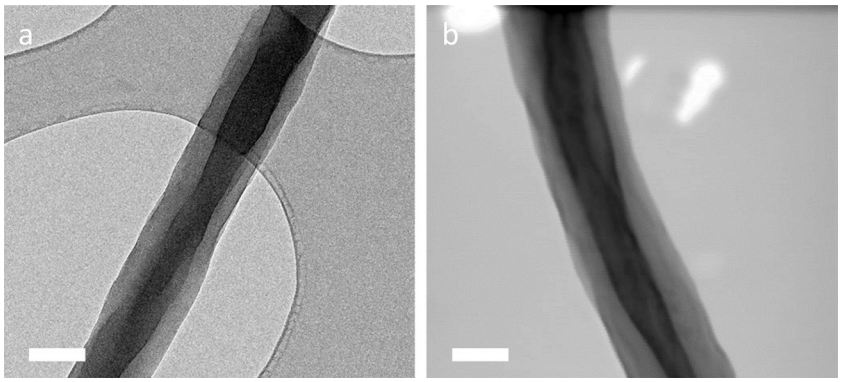

Fig. 3 TEM images of core–shell nanofibers. (a) R-PAN nanofibers. (b) C-PAN nanofibers. The scale bar is 200 nm.

3.2. Thermogravimetric analysis (TGA) and derivative thermogravimetry (DTG)

To determine the amount of core or shell material injected into each nanofiber, TGA and DTG measurements were conducted, *cf.* Fig. 4.[29,30] By comparing TGA results (Fig. 4a) and the phase transition temperatures in the DTG results (Fig. 4b), once can determine the weight losses of the materials in question. In the temperature range of 0–800 °C, the weight losses of pristine PAN, cure, and resin in the nanofibers were 52, 24, and 8%, respectively, consistent with the previous studies.[29,39,40] The weight loss of cure was higher than that of resin because the resin volume encapsulated in the R-PAN nanofiber was smaller than the cure volume encapsulated in the C-PAN nanofibers, because the resin was mixed with *n*-hexane for stable co-electrospinning, as mentioned in section 2.2. Because of the high evaporation rate of *n*-hexane, most *n*-hexane evaporated before samples for thermal analysis were prepared. Therefore, *n*-hexane was not detected in the TGA results, *i.e.* no weight loss corresponding to *n*-hexane was detected (not shown here). Fig. 4 also shows the results for the mutually entangled R-PAN and C-PAN nanofiber mats, which are denoted as RC-PAN nanofibers.

3.3. Transmittance

The application of such self-healing nano-textured coatings to optical devices (such as opto-electric sensors, solar cells, displays, and electronic touch screens) is important to enhance the sustainability and to hasten the development of the next-generation devices. However, co-electrospun polymer nanofiber mats are generally white in color with low optical transmittance, because of the light-scattering effect caused by the nano-scale non-woven structure of the nanofibers commensurate with the wavelength of light. Accordingly, typical self-healing core–shell nanofiber mats or films have poor optical properties.

However, the optical properties of self-healing core–shell nanofibers can be improved by embedding the nanofibers into a transparent composite layer, such as PDMS and epoxy-based negative photoresist SU-8, as demonstrated in our previous studies.[29,41] First, both the R-PAN and C-PAN nanofibers were co-electrospun onto a substrate (*i.e.* an ITO glass and a steel substrate) attached on a drum collector (Fig. 1). Next, a proper amount of liquid PDMS was poured onto the RC-PAN nano-

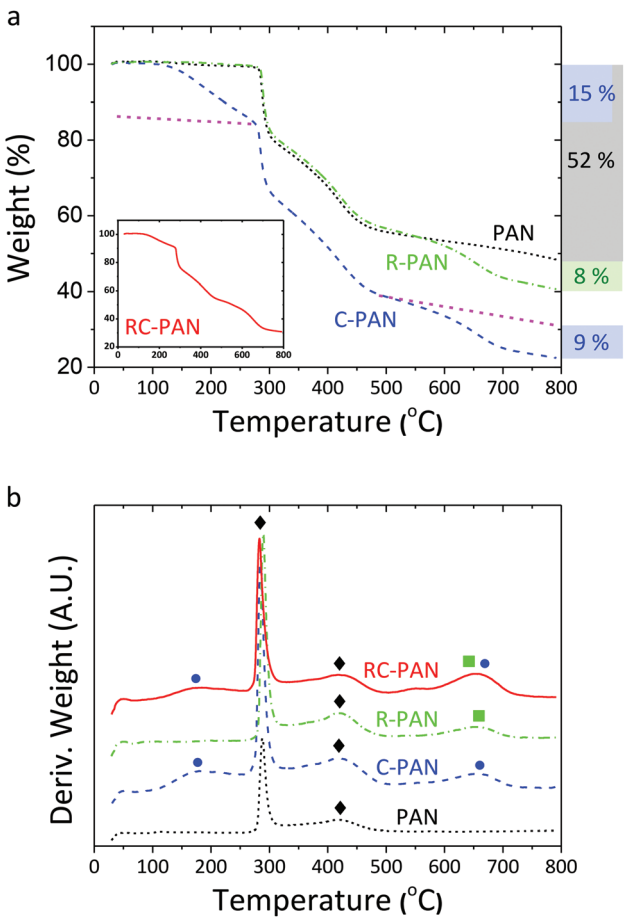

Fig. 4 Thermal analysis of PAN, R-PAN, C-PAN, and RC-PAN nanofibers. (a) TGA curves. The right-hand column lists the total weight loss of the core and shell materials within the nanofibers (gray: PAN, green: resin monomer, blue: cure, and purple line is added for estimating the weight loss of cure). Inset graph shows the TGA results for RC-PAN fiber mats. (b) DTG curves. The phase transition temperatures of the core and shell materials are marked (black diamonds at 288, 420 °C: PAN; green rectangles at 660 °C: resin monomer; blue circles at 180, 660 °C: cure).

fiber-coated substrate. Finally, the composite film was dried to permit solidification at room temperature for 48 h (although the solidification time can be decreased to a few hours by adjusting the drying temperature to above 70 °C). Fig. 5a shows the transmittance (T) values of the RC-PAN nanofiber-embedded composites on an ITO substrate compared to pristine PDMS on ITO (T = 100% in the latter case). T for 550 nm light is decreased from 90 to 10% as the deposition time t_{dep} is increased from 5 to 120 min. The deposited amount of RC-PAN nanofibers for t_{dep} = 5 min is only 1.065 μL on the substrate size of 3 × 3 cm^2. And the poured PDMS amount is 458.37 μL on that of size. That is, 0.23% [= (1.065/458.37) × 100] is the loading percentage of t_{dep} = 5 min case. Although such a few RC-PAN nanofibers were embedded in the case of t_{dep} = 5 min (T = 93%) (Fig. 5b), the self-healing composite revealed sufficient ability to protect the base substrate from corrosion, as described in the following section. Note that T can be increased not only by shortening the deposition time but also by reducing the embedded fiber diameter as our previous study (not studied here) where PAN nanofiber-embedded SU-8 composite was studied for LED and OLED application.[41] Furthermore, this self-healing nanofiber-embedded composite can be used without a substrate by detaching the composite from the latter, as shown in Fig. 5e. As depicted in Fig. 5f and g, the nanofibers containing healing agents are well-entangled in the PDMS layer, and are capable of repairing any microcracks regardless of crack size and propagation direction, in distinction from the capsule-type self-healing composites. In

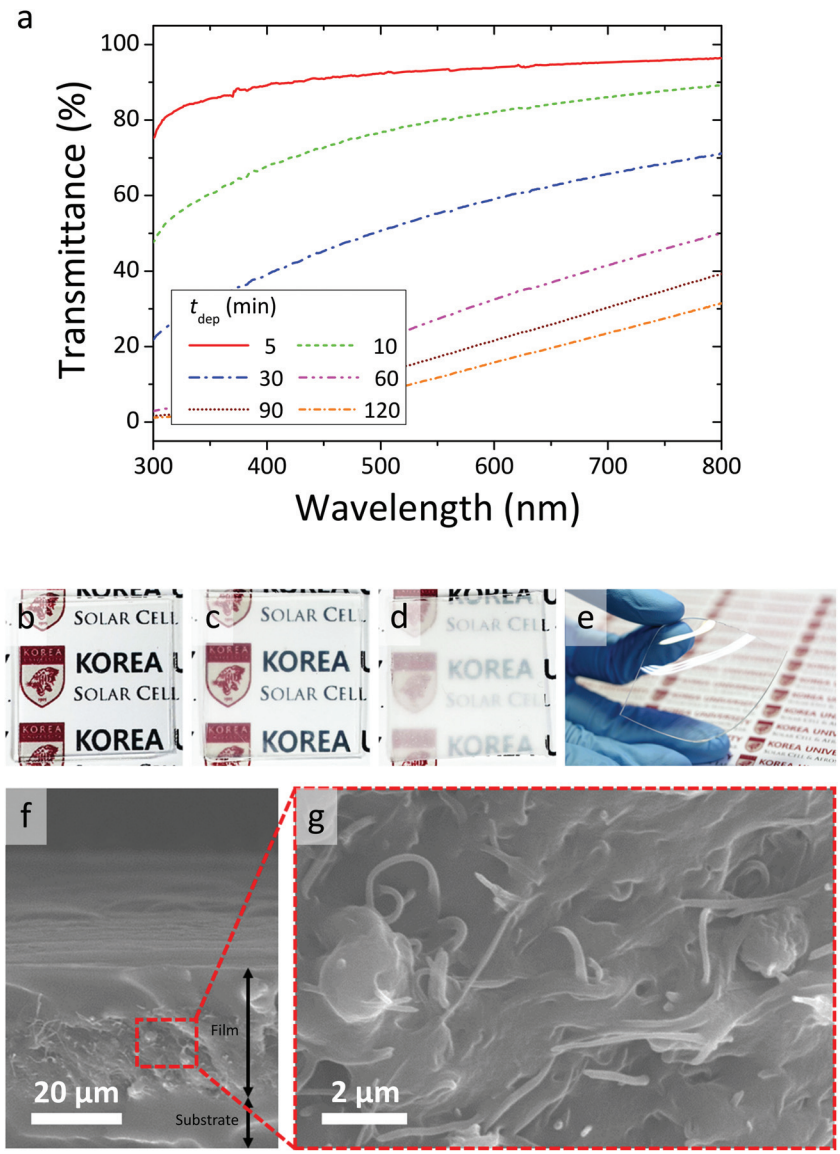

Fig. 5 (a) Transmittance *versus* wavelength of the RC-PAN nanofiber-embedded composite film on ITO glass; photographs of films at different deposition times t_{dep}: (b) t_{dep} = 5 min, (c) t_{dep} = 30 min, and (d) t_{dep} = 120 min. (e) Photograph of the flexible transparent self-healing composite removed from the ITO substrate (t_{dep} = 5 min). (f, g) Cross-sectional SEM images of the composite film (t_{dep} = 120 min).

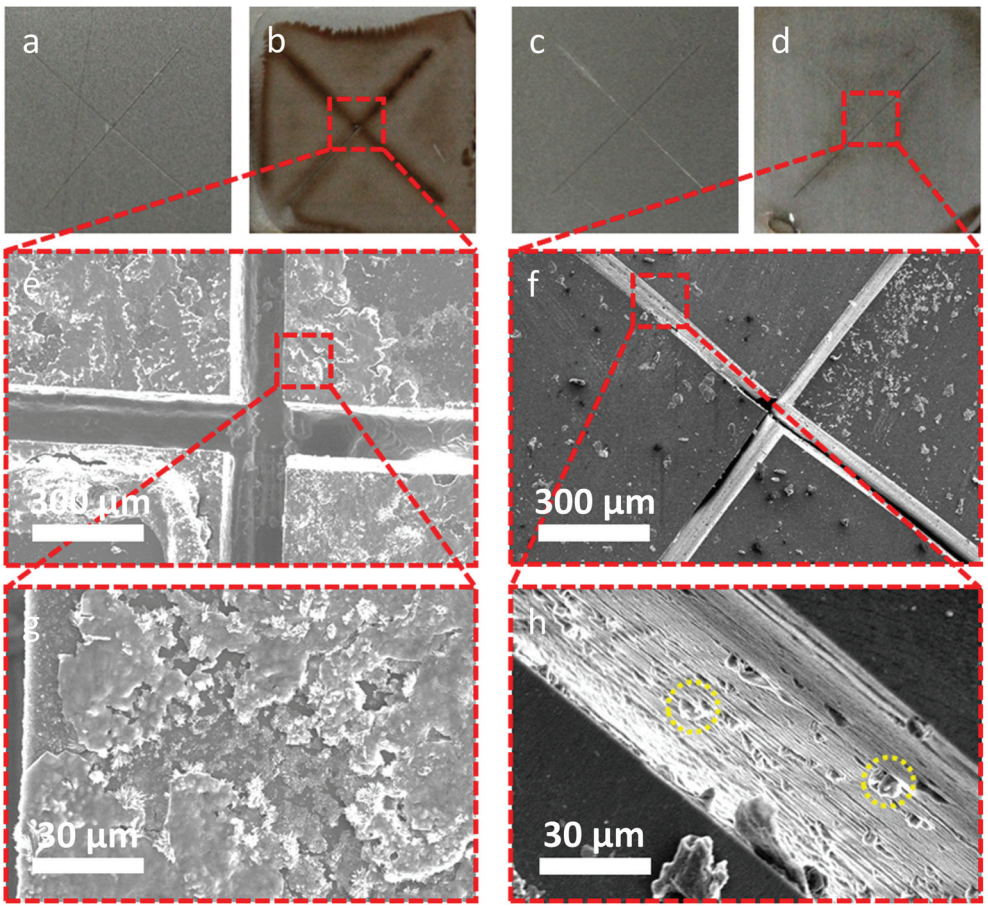

Fig. 6 Corrosion test images associated with the presence of the RC-PAN nanofibers in the composite layer on a steel substrate. Corrosion test images of (a, b) t_{dep} = 0 min (scratched metal with pristine PDMS coating), (c, d) t_{dep} = 5 min (metal with nanofiber-composite coating). Samples shown as time passed: (a, c) 0 min and (b, d) 60 min. SEM images of the tested samples for (e, g) t_{dep} = 0 min and (g, h) t_{dep} = 5 min.

the latter case, the reparability of micro-cracks is limited because it is hard to disperse the capsules uniformly and cracks can propagate in the spaces between them.[21,42,43]

3.4. Self-healing performance

Fig. 6 shows the corrosion test results of the pristine PDMS and the self-healing core–shell nanofiber-embedded composite, both deposited on steel substrates. All films were scratched deeply with crossed lines using a knife. After that, the samples were left for 48 h. Then, an acetic acid solution was poured onto the films. In contrast to the pristine PDMS case, in which complete corrosion occurs (Fig. 6b, e and g), the self-healing composite exhibits perfect anti-corrosive performance (rusting prevention) (Fig. 6d, f and h) after both coatings were damaged. Note that clots, indicated by yellow dashed circles in Fig. 6h, result from polymerization of the released resin monomer in the presence of the released cure, which is also evident in the SEM images in Fig. 5f and g.

In addition to anti-corrosive performance, electric-insulation performance is also important for practical industrial applications.[44–46] For this reason, we conducted an electrochemical test to better characterize the insulating performance of our self-healing composite, as shown in Fig. 7 and 8. The pristine PDMS and self-healing composites were prepared on steel substrates with different deposition times; all samples were identically scratched as depicted in Fig. 7a. After 48 h, open-bottomed cylinders were placed on the samples with no gaps between the edge of the holes and the samples. The cylinders were filled with acetic acid as an electrolyte (Fig. 7b). Electric wires from a current measurement device were directly connected to the electrolyte and the base of the steel substrate, respectively. As depicted in Fig. 7c, the self-healed sample forms a protective layer between the steel and the electrolyte. However, the pristine PDMS does not offer this protection, and indeed, these results are confirmed through the electrochemical test, as plotted in Fig. 8. The pristine PDMS (t_{dep} = 0 min) yields an electrical current of 10–25 mA, indicating the exposure of the base steel substrate to the electrolyte because of the absence of the self-healing phenomenon. Meanwhile, perfect electrical insulation, demonstrated by a current of 0 mA, is exhibited by self-healing composites with $t_{dep} \geq$ 30 min. (R2-2) A non-zero current was detected in the case of t_{dep} = 5 and 10 min (not shown). This indicates that $t_{dep} \leq$ 10 min is not sufficient to create an intact anti-corrosive

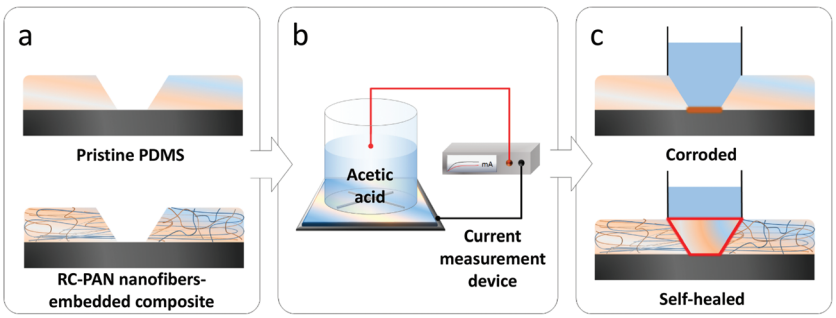

Fig. 7 Electrochemical test. (a) Scratched composite films on steel substrates. (b) Schematic of the electrochemical test setup. (c) The tested samples.

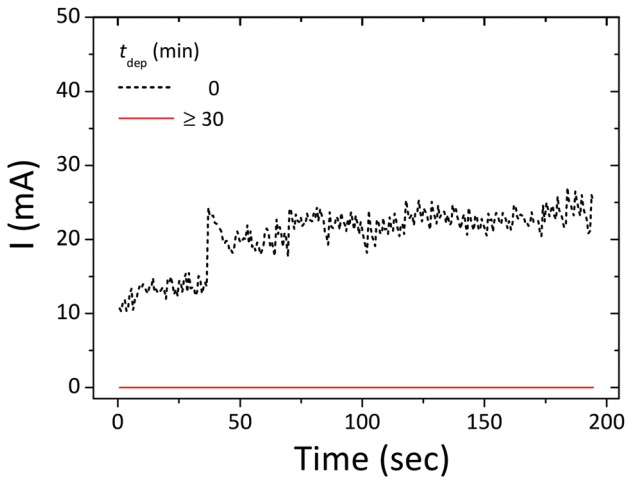

Fig. 8 Results of electrochemical test with RC-PAN nanofiber-embedded composite film with different deposition times t_{dep} on steel substrates (the current, $I \rightarrow 0$ mA for $t_{dep} \geq 30$ min cases, for which all straight lines are overlaid one to another as all of their current values approach to zero, indicating the complete electrical insulation with self-healed materials).

coating, and $t_{dep} \geq 30$ min is required to fabricate a coating with both anti-corrosive and electrically insulating properties.

4. Conclusion

Coaxial electrospinning was shown to be capable of forming dual mutually-entangled nanofiber mats comprised of core–shell nanofibers with healing agents with either liquid dimethylvinyl-terminated dimethyl siloxane (resin monomer), or methylhydrogen dimethyl siloxane cure in the core. Being embedded in transparent matrices, either PDMS or SU-8, these core–shell nanofiber mats formed flexible transparent self-healing composites. Their light transmittance in the 400–800 nm wavelength band was about 90%. Being deposited on metal surface, these composites created an anti-corrosive barrier. When this barrier was scratched, it revealed self-healing properties, *i.e.* the resin monomer and cure released from the fiber cores, polymerized and restored integrity of the barrier. The self-healed was being able to protect metal surface underneath from corrosion, when submerged into acetic acid.

Acknowledgements

This work was primarily supported by the International Collaboration Program funded by the Agency for Defense Development. This work was partially supported by ISTDP (10045221), GFHIM (NRF-2013M3A6B1078879), and NRF-2013R1A2A2A05005589. The authors extend their appreciation to the Deanship of Scientific Research at King Saud University for its funding this Prolific Research group (PRG-1436-03).

References

1 G. H. Koch, M. P. Brongers, N. G. Thompson, Y. P. Virmani and J. H. Payer, *Corrosion cost and preventive strategies in the United States*, 2002.
2 K. Riefsnider, K. Schulte and J. Duke, *ASTM STP*, 1983, **813**, 136–159.
3 I. Reimanis, *Mater. Sci. Eng., A*, 1997, **237**, 159–167.
4 E. Brooman, *Met. Finish.*, 2002, **100**, 48–53.
5 M. L. Zheludkevich, D. G. Shchukin, K. A. Yasakau, H. Möhwald and M. G. Ferreira, *Chem. Mater.*, 2007, **19**, 402–411.
6 S. R. White, N. Sottos, P. Geubelle, J. Moore, M. R. Kessler, S. Sriram, E. Brown and S. Viswanathan, *Nature*, 2001, **409**, 794–797.
7 J. D. Rule, N. R. Sottos and S. R. White, *Polymer*, 2007, **48**, 3520–3529.
8 S. H. Cho, S. R. White and P. V. Braun, *Adv. Mater.*, 2009, **21**, 645–649.
9 C. J. Hansen, W. Wu, K. S. Toohey, N. R. Sottos, S. R. White and J. A. Lewis, *Adv. Mater.*, 2009, **21**, 4143–4147.
10 J. H. Park and P. V. Braun, *Adv. Mater.*, 2010, **22**, 496–499.
11 P. A. Sørensen, S. Kiil, K. Dam-Johansen and C. Weinell, *J. Coat. Technol. Res.*, 2009, **6**, 135–176.

12 M. W. Keller, S. R. White and N. R. Sottos, *Adv. Funct. Mater.*, 2007, **17**, 2399–2404.
13 Y. C. Yuan, M. Z. Rong, M. Q. Zhang, J. Chen, G. C. Yang and X. M. Li, *Macromolecules*, 2008, **41**, 5197–5202.
14 S. H. Cho, H. M. Andersson, S. R. White, N. R. Sottos and P. V. Braun, *Adv. Mater.*, 2006, **18**, 997–1000.
15 T. S. Coope, D. F. Wass, R. S. Trask and I. P. Bond, *Macromol. Mater. Eng.*, 2014, **299**, 208–218.
16 Y.-K. Song, Y.-H. Jo, Y.-J. Lim, S.-Y. Cho, H.-C. Yu, B.-C. Ryu, S.-I. Lee and C.-M. Chung, *ACS Appl. Mater. Interfaces*, 2013, **5**, 1378–1384.
17 T. S. Coope, U. F. Mayer, D. F. Wass, R. S. Trask and I. P. Bond, *Adv. Funct. Mater.*, 2011, **21**, 4624–4631.
18 M. Krogsgaard, M. A. Behrens, J. S. Pedersen and H. Birkedal, *Biomacromolecules*, 2013, **14**, 297–301.
19 D. Therriault, R. F. Shepherd, S. R. White and J. A. Lewis, *Adv. Mater.*, 2005, **17**, 395–399.
20 S. Sinha-Ray, D. Pelot, Z. Zhou, A. Rahman, X.-F. Wu and A. L. Yarin, *J. Mater. Chem.*, 2012, **22**, 9138–9146.
21 X. F. Wu, A. Rahman, Z. Zhou, D. D. Pelot, S. Sinha-Ray, B. Chen, S. Payne and A. L. Yarin, *J. Appl. Polym. Sci.*, 2013, **129**, 1383–1393.
22 A. L. Yarin, S. Sinha-Ray and B. Pourdeyhimi, *Polym.*, 2011, **52**, 2929–2938.
23 R. Ma, J. Lee, D. Choi, H. Moon and S. Baik, *Nano Lett.*, 2014, **14**, 1944–1951.
24 B. Vazquez, H. Vasquez and K. Lozano, *Polym. Eng. Sci.*, 2012, **52**, 2260–2265.
25 Y. Rane, A. Altecor, N. S. Bell and K. Lozano, *J. Eng. Fibers Fabr.*, 2013, **8**, 88–95.
26 X. Zhuang, X. Yang, L. Shi, B. Cheng, K. Guan and W. Kang, *Carbohydr. Polym.*, 2012, **90**, 982–987.
27 A. M. Behrens, B. J. Casey, M. J. Sikorski, K. L. Wu, W. Tutak, A. D. Sandler and P. Kofinas, *ACS Macro Lett.*, 2014, **3**, 249–254.
28 D. H. Reneker and A. L. Yarin, *Polym.*, 2008, **49**, 2387–2425.
29 M. W. Lee, S. An, C. Lee, M. Liou, A. L. Yarin and S. S. Yoon, *J. Mater. Chem. A*, 2014, **2**, 7045–7053.
30 M. W. Lee, S. An, C. Lee, M. Liou, A. L. Yarin and S. S. Yoon, *ACS Appl. Mater. Interfaces*, 2014, **6**, 10461–10468.
31 D.-G. Yu, G. R. Williams, X. Wang, X.-K. Liu, H.-L. Li and S. A. Bligh, *RSC Adv.*, 2013, **3**, 4652–4658.
32 Y.-H. Wu, D.-G. Yu, X.-Y. Li, A.-H. Diao, U. E. Illangakoon and G. R. Williams, *J. Mater. Sci.*, 2015, **50**, 3604–3613.
33 X. Wang, D.-G. Yu, X.-Y. Li, S. A. Bligh and G. R. Williams, *Int. J. Pharm.*, 2015, **490**, 384–390.
34 H. Isaacs, *Corros. Sci.*, 1988, **28**, 547–558.
35 M. Ishikawa, S. Yoshitake, M. Morita and Y. Matsuda, *J. Polym. Res.*, 1994, **141**, L159–L161.
36 S. Reznik, A. Yarin, E. Zussman and L. Bercovici, *Phys. Fluids*, 2006, **18**, 062101.
37 D. H. Reneker, A. L. Yarin, H. Fong and S. Koombhongse, *J. Appl. Phys.*, 2000, **87**, 4531–4547.
38 A. L. Yarin, B. Pourdeyhimi and S. Ramakrishna, *Fundamentals and Applications of Micro and Nanofibers*, Cambridge University Press, 2014.
39 T. J. Xue, M. A. McKinney and C. A. Wilkie, *Polym. Degrad. Stab.*, 1997, **58**, 193–202.
40 W.-x. Zhang, Y.-z. Wang and C.-f. Sun, *J. Polym. Res.*, 2007, **14**, 467–474.
41 H. J. Lee, S. An, J. H. Hwang, S.-G. Jung, H. S. Jo, K. N. Kim, Y. S. Shim, C. H. Park, S. S. Yoon and Y. W. Park, *ACS Appl. Mater. Interfaces*, 2014, **7**, 68–74.
42 S. H. Boura, M. Peikari, A. Ashrafi and M. Samadzadeh, *Prog. Org. Coat.*, 2012, **75**, 292–300.
43 H. Jin, C. L. Mangun, D. S. Stradley, J. S. Moore, N. R. Sottos and S. R. White, *Polym.*, 2012, **53**, 581–587.
44 C. Calebrese, L. Hui, L. S. Schadler and J. K. Nelson, *IEEE Trans. Dielectr. Electr. Insul.*, 2011, **18**, 938–945.
45 J. Castellon, H. Nguyen, S. Agnel, A. Toureille, M. Frechette, S. Savoie, A. Krivda and L. Schmidt, *IEEE Trans. Dielectr. Electr. Insul.*, 2011, **18**, 651–658.
46 T. Morishita, M. Matsushita, Y. Katagiri and K. Fukumori, *J. Mater. Chem.*, 2011, **21**, 5610–5614.